ADVANCED ENERGY MATERIALS
www.advenergymat.de

Molecular Level Insight into Enhanced n-Type Transport in Solution-Printed Hybrid Thermoelectrics

*Edmond W. Zaia, Madeleine P. Gordon, Valerie Niemann, Jaeyoo Choi, Ruchira Chatterjee, Chih-Hao Hsu, Junko Yano, Boris Russ, Ayaskanta Sahu, and Jeffrey J. Urban**

Perylene diimide (PDI) derivatives hold great promise as stable, solution-printable n-type organic thermoelectric materials, but as of yet lack sufficient electrical conductivity to warrant further development. Hybrid PDI-inorganic nanomaterials have the potential to leverage these physical advantages while simultaneously achieving higher thermoelectric performance. However, lack of molecular level insight precludes design of high performing PDI-based hybrid thermoelectrics. Herein, the first explicit crystal structure of these materials is reported, providing previously inaccessible insight into the relationship between their structure and thermoelectric properties. Allowing this molecular level insight to drive novel methodologies, simple solution-based techniques to prepare PDI hybrid thermoelectric inks with up to 20-fold enhancement in thermoelectric power factor over the pristine molecule (up to 17.5 μW mK^{-2}) is presented. This improved transport is associated with reorganization of organic molecules on the surface of inorganic nanostructures. Additionally, outstanding mechanical flexibility is demonstrated by fabricating solution-printed thermoelectric modules with innovative folded geometries. This work provides the first direct evidence that packing/organization of organic molecules on inorganic nanosurfaces is the key to effective thermoelectric transport in nanohybrid systems.

1. Introduction

Flexible thermoelectric devices can realize energy generation or solid-state heating/cooling devices with conformal geometries, enabling a new portfolio of applications for thermoelectric technologies.[1] As personal electronic devices become increasingly ubiquitous, interest in flexible thermoelectric devices for portable, renewable energy generation and localized cooling, particularly in wearable technologies, has surged.[2–4] Propelled by the emergence of new classes of organic semiconductors, polymers, and organic–inorganic composites over the past few years, several flexible thermoelectric devices capable of power generation have been successfully demonstrated.[5–7] These soft thermoelectric materials are rapidly catching up to their inorganic counterparts in terms of thermoelectric efficiency, while leveraging significant advantages from a processing standpoint.[8–10] In general, solution-processed soft thermoelectrics open the door to a variety of new thermoelectric applications due to flexible form factors and scalable, roll-to-roll fabrication techniques without the need for costly energy-intensive processing steps.[11]

The performance of a thermoelectric material is often evaluated using the dimensionless figure of merit, $ZT = S2\sigma T/\kappa$, which encompasses three material properties: the Seebeck coefficient or thermopower (S), electrical conductivity (σ), and thermal conductivity (κ). Fabricating a commercially viable thermoelectric module requires both high performing p-type (hole transporting) and n-type (electron transporting) materials, which are connected electrically in series and thermally in parallel. Recent work in soft thermoelectrics has seen impressive progress in improving power factors in this class of materials. However, there is a striking scarcity of high performing n-type soft materials due to poor electron transport properties and insufficient stability in ambient conditions.[1,3]

State of the art organic n-type materials include organometallic poly(metal 1,1,2,2-ethenetetrathiolate) derivatives, which have demonstrated power factors up to 66 μW mK^{-2}, but these materials rely on solid-state powder processing, making them unfavorable from a processing standpoint.[12] To avoid the challenges and costs of solid-state processing, focus has shifted to

E. W. Zaia
Department of Chemical and Biomolecular Engineering
University of California
Berkeley, CA 94720, USA
E. W. Zaia, M. P. Gordon, V. Niemann, J. Choi, C.-H. Hsu, B. Russ, A. Sahu, J. J. Urban
The Molecular Foundry
Lawrence Berkeley National Laboratory
Berkeley, CA 94720, USA
E-mail: jjurban@lbl.gov
M. P. Gordon
Applied Science and Technology Graduate Group
University of California
Berkeley, CA 94720, USA
R. Chatterjee, J. Yano
Department of Chemical and Biomolecular Engineering
Lawrence Berkeley National Laboratory
CA 94720, USA
A. Sahu
Department of Chemical Engineering
New York University
NY 11201, USA
The ORCID identification number(s) for the author(s) of this article can be found under https://doi.org/10.1002/aenm.201803469.

DOI: 10.1002/aenm.201803469

solution-processed materials. Within this family of solution-processed thermoelectric materials, doped single-walled carbon nanotubes and halogenated benzodifurandione-based oligo (p-phenylene vinylene) (BDPPV) derivatives have achieved power factors up to 18 and 28 μW mK^{-2}, respectively.[13,14] Of particular interest are small molecules such as perylene diimide (PDI) derivatives which exhibit good electronic conductivity, air stability, water solubility, and tunability of both electronic and optical properties.[15,16] PDIs have been used as pigments since the 1950s, and are therefore inexpensive to synthesize at large scale. Self-doped PDIs have been reported to achieve up to 1.4 μW mK^{-2} power factors, a good starting point for materials development but too low to be of practical use at the present.[15,17] Such materials are exceptionally attractive in the effort to realize solution-printed thermoelectrics for wearable and personal electronic application, but even greater power factors are needed.

Hybrid organic–inorganic materials have been identified as a particularly promising path toward next generation n-type soft thermoelectrics due to their ability to realize performances exceeding that of either individual constituent while still leveraging the unique advantages of soft thermoelectrics.[18] For example, a composite formed from 2D TiS_2 nanosheets with C_{60} nanoparticles was shown to achieve a ZT as high as 0.3 at 400 K (a power factor of ≈375 μW mK^{-2}), exceeding the reported ZT values for either individual component.[19,20] While this result highlights the potential of organic–inorganic composites to realize impressive thermoelectric performance, hybrid materials of this sort require multistep, energy intensive fabrication processes including high-temperature, low-pressure synthesis (640 °C for 3 days) and solid-state ball milling. In order to develop commercially relevant materials, there is a strong need to innovate versatile techniques for the production of n-type thermoelectrics using solely low-temperature, solution-based operations compatible with ambient conditions.

Moreover, while it is known that the organic/inorganic interface plays a key role in the high performance of these composites, lack of detailed structural data and insufficient contrast at the organic/inorganic interface has stymied efforts to conclusively elucidate the mechanisms behind such performance enhancements. Current state-of-the-art in this material class has implicated physical phenomena such as interfacial transport, structural/morphologic effects, and modification of the energy dependence of carrier scattering, or energy filtering, in these thermoelectric trends.[21–26] Recent work has suggested that the role of energy filtering has been overstated in this field, and instead structural/morphological effects and interfacial charge transfer at the organic–inorganic interface are largely responsible for enhanced thermoelectric performance in hybrid materials.[27,28] For example, it was reported that, in composites of tellurium nanowires (Te NWs) and poly(3,4-ethylenedioxythiophene):poly(styrene sulfonate) (PEDOT:PSS), the organic component self-assembled into an ordered structure at the surface of the inorganic nanostructure, creating a region of high local ordering and contributing to enhanced carrier transport. However, investigation of this so-called templating effect of the organic component on the inorganic surface has thus far been theoretical, driven by molecular dynamics and density functional theory. Directly probing the hard-soft interface in hybrid materials is challenging, and thus experimental observation of this templating effect remains elusive.

In this article, we present a novel, versatile approach to prepare stable n-type hybrid thermoelectrics using low-temperature, ambient techniques, while simultaneously providing new insight into the mechanism behind high performance in organic–inorganic hybrid thermoelectrics. PDIs were used as the organic component due to their large scale and inexpensive synthesis, electronic conductivity, solution processability, chemical tunability, and air stability.[15,29] Te NWs were chosen as the inorganic component. Te NWs are a well-studied prototypical thermoelectric material, capable of being synthesized at large scale and doped either n- or p-type.[25,30] Recent work has shown that Te NWs are amenable to platform ligand exchange techniques, providing a methodological precedent for forming PDI-Te composites.[21] Additionally, it has been shown that the Te nanowire surface can act as a structural template for conductive polymer ligands, generating locally high conductivity at the hard-soft interface.[27] Both components in this hybrid system can be synthesized at scale using low temperature, solution-based techniques and produce air-stable films. Furthermore, the two components are likely to be energetically compatible, with only a slight offset in their work functions (WFs) as determined via ultraviolet photoelectron spectroscopy (UPS) (**Table 1**). In this work, we develop a new approach to preparing high performance PDI-Te hybrid thermoelectrics. We first apply the current literature state-of-the-art hybrid preparation methodology (for simplicity, this method will hence be called Method A), and perform detailed investigation of the structural and energetic properties of the composites. Notably, we provide the first explicit solution for the crystal structure of these materials, allowing us to fill a critical gap in the literature and tie molecular level information to the observed trends in thermoelectric performance of these materials. Driven by new physical understanding of the material system, the hybrid preparation methodology is revisited, and a second methodology is developed (we will refer to this as Method B). Utilizing this new approach, we prepare PDI-Te composites that are able to achieve up to 20-fold enhancement in the thermoelectric power factor over pure PDI films. Moreover, the detailed investigation of the structural and energetic properties of the composites provides the opportunity to directly relate molecular level phenomena to macroscopic performance metrics, providing key understanding previously missing in the literature and informing future work on organic–inorganic composite systems for thermoelectric and electronic applications. Finally, we demonstrate that this approach is compatible with next-generation flexible thermoelectric applications by fabricating solution-printed thermoelectric generators (TEGs) with flexible and novel architectures.

Table 1. WF and IE for PDI-Te composites with varying PDI content prepared via Method A, as determined by UPS.

	WF [eV]	IE [eV]
S-Te (0% PDI)	3.7	4.1
10% PDI	4.2	4.5
90% PDI	3.7	4.2
100% PDI	3.8	4.3

2. Results and Discussion

2.1. Thermoelectric Characterization (Method A)

Following a previously published platform methodology (Method A), PDI-capped Te nanowires (PDI-Te NWs) were first prepared via a ligand exchange technique, in which sulfur is used as a linker molecule to mediate binding between the Te and PDI domains (**Figure 1**a). Full synthetic details are provided in the experimental section. Method A represents an intuitive approach extending a current state-of-the-art technique from the literature, shown to be broadly effective in producing a variety of organic–inorganic composites.[21] PDI-Te composites were prepared at a variety of compositions, and their thermoelectric, structural, and electronic properties investigated.

We first examine the effect of composition on thermoelectric performance of PDI-Te composites prepared via Method A. **Figure 2**a depicts the electrical conductivity and Seebeck coefficient of PDI-Te composites prepared via Method A with varying PDI content. Significantly, we observe nonmonotonic trends in both the Seebeck coefficient and the electrical conductivity. Such a trend necessitates some hybridizing interaction between the organic and inorganic phases in the composite films; otherwise, standard effective medium theory would predict that the composite performance should lie intermediate between that of the pure components.[18] These nonmonotonic trends were reproduced over five independent syntheses. It is also important to note that the thermoelectric performance of these hybrid films exceed that of either starting materials, a result with important implications for the design of hybrid thermoelectric devices. In PDI-Te composites prepared via Method A, the thermoelectric power factor is enhanced greater than sixfold over pure PDI, driven by increased electrical conductivity in the high PDI regime. Clearly, it is critical to understand the nature of this performance enhancement in order to provide insight for next-generation hybrid thermoelectric material design.

In order to investigate this phenomenon, we consider the conductivity of a material, which can be written as:

$$\sigma = ne\mu$$

where the electrical conductivity (σ) is a function of the charge carrier density (n) and mobility (μ), where e is the elementary charge. Thus, the improved conductivity of these films must be the result of either doping of additional free carriers into the system or increased carrier mobility. On the other hand, nonmonotonic trends in the Seebeck coefficient of composite semiconductors can be the result of many factors, such as doping/dedoping, shifts in the slope of the density of states, and energy-dependent scattering phenomena.[25,31] In order

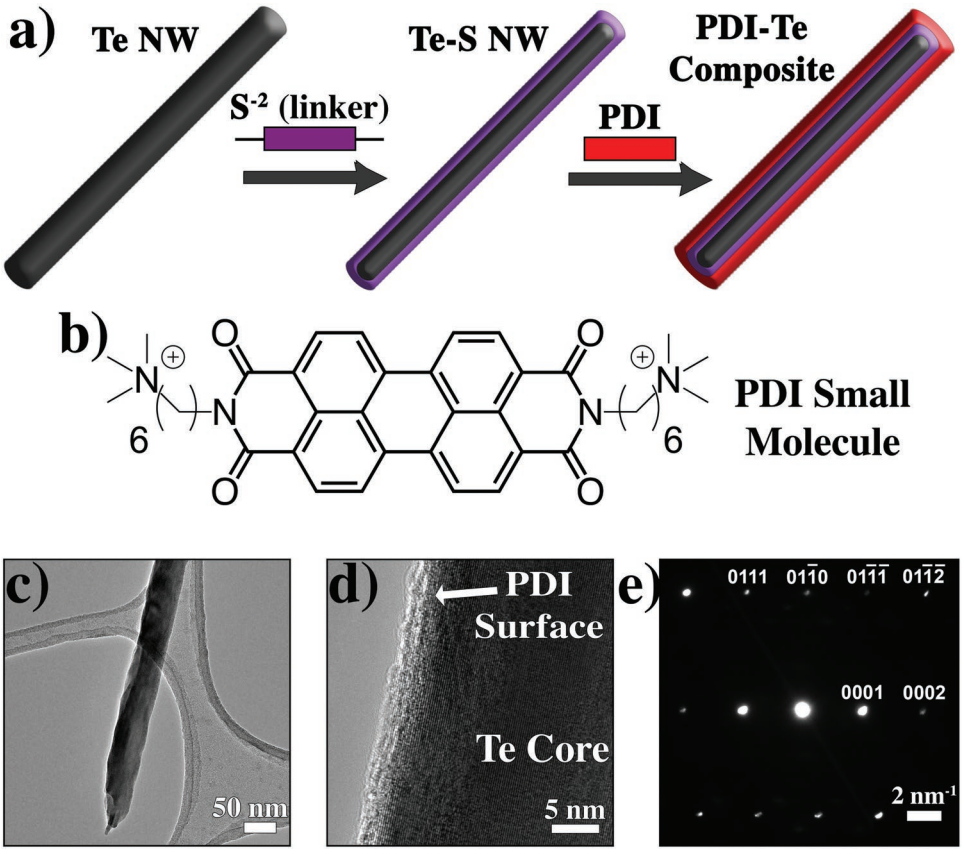

Figure 1. a) Cartoon depiction of platform-based design scheme for n-type hybrid nanostructures, Method A. b) Chemical structure of PDI small molecule with high thermoelectric properties. c) TEM depicts high quality, single crystal Te nanowires. d) HRTEM reveals functional organic layer has successfully been strongly adhered to inorganic nanowire core. e) SAED confirms inorganic core is single-crystalline Te.

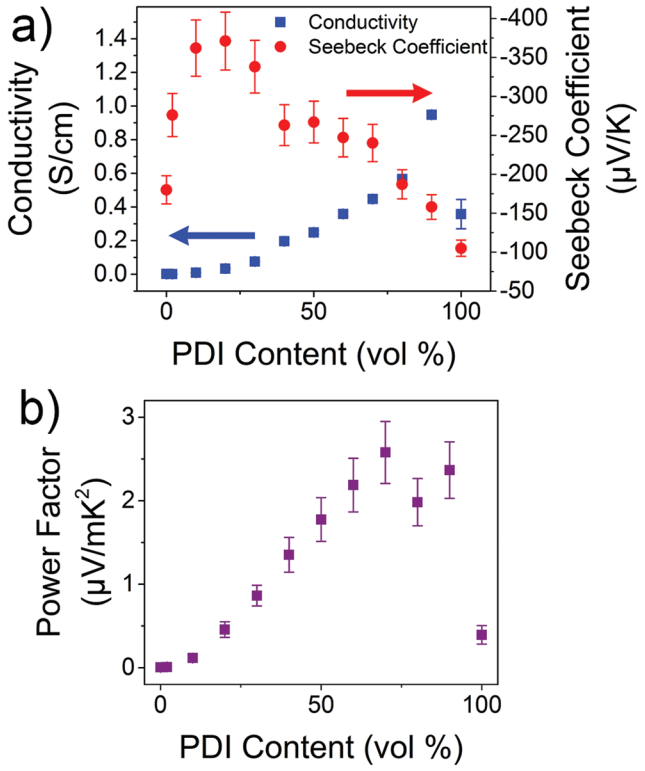

Figure 2. PDI-Te composite nanostructures prepared via Method A demonstrate enhanced thermoelectric performance relative to pure components. a) Significantly, nonmonotonic trends are observed in both electrical conductivity and Seebeck coefficient. These phenomena are reproducible over five separate experiments. b) PDI-Te composites demonstrate up to sixfold improvement in power factors in the high PDI regime.

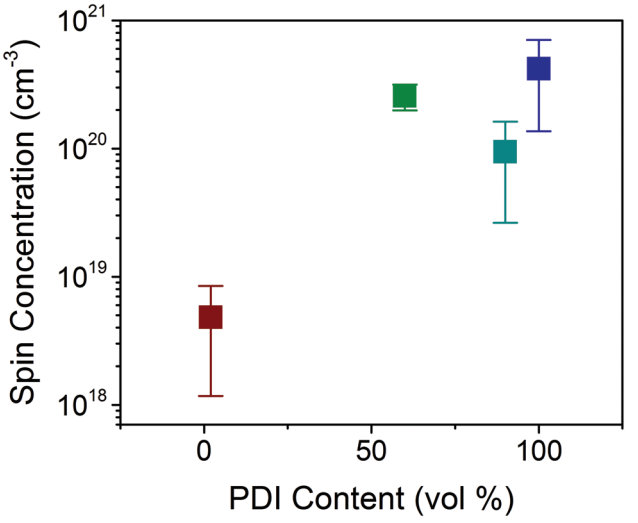

Figure 3. EPR measurements allow quantification of unpaired spin concentration in samples with varying PDI content prepared via Method A. While high PDI composites demonstrate enhanced conductivity relative to pure PDI, they surprisingly demonstrate slightly reduced spin concentrations, suggesting that doping is not the key factor in the nonmonotonic conductivity trends observed in this regime.

to elucidate the physical origin of the nonmonotonic trends in the composite electrical conductivity and Seebeck coefficient and, in turn, the improved thermoelectric performance in hybrid PDI thermoelectrics, each of these factors is investigated.

2.2. Quantitation of Carrier Concentration

A parameter key to both electrical conductivity and Seebeck coefficient is the concentration of conductive charge carriers. Several groups have observed self-doping effects in similar PDI systems, and similar doping effects could be responsible for the enhanced electrical conductivity in the hybrid films with high PDI content. In order to test this hypothesis, both ultraviolet–visible–near infrared absorption (UV–vis–NIR) and electron paramagnetic resonance (EPR) were performed on hybrid films of varying PDI content. UV–vis–NIR absorption spectra depict the expected optical transitions in the visible range, with three characteristic peaks representative of PDI polaron charge carriers (≈730, 800, 1100 nm), consistent with previous literature (Figure S1, Supporting Information).[15,32,33] The spectra are quite similar for all films in the high PDI regime, which is not suggestive of significant changes in carrier concentration. Further corroborating this conclusion, the charge carrier densities in the composite films all appear to be of the same order of magnitude in the high PDI regime, as quantified by EPR (**Figure 3**).[34–36] In fact, composites with high PDI content, which exhibit enhanced electrical conductivities relative to pure PDI, actually demonstrate slightly reduced carrier concentrations. Films with low PDI content show significantly lower spin concentrations, suggesting that PDI acts as both stabilizing ligand and active dopant in this system. We also note that the doping levels in these films are quite high, consistent with previous reports.[15,32] Combined, these data indicate that changes in the carrier concentration cannot be solely responsible for the increased electrical conductivity and subsequent improvement in thermoelectric performance observed in the hybrid films. Instead, these phenomena must be the result of changes in the apparent thin film electron mobility. That is, the addition of inorganic nanostructures influences the thermoelectric performance of hybrid films through a mobility channel. To further illustrate this point, the carrier mobilities of the PDI-Te thin films with varying PDI content have been extracted from this EPR data and plotted (Figure S2, Supporting Information). A peak is clearly observed in the high PDI regime, coincident with the enhanced electrical conductivity and thermoelectric power factor observed in this hybrid system. Moreover, Hall measurements were performed to independently probe the carrier mobilities in the same PDI-Te thin films, demonstrating an identical trend to the EPR approach (Figure S2, Supporting Information). Both approaches independently corroborate the conclusion that increased carrier mobility in the high PDI regime is responsible for the enhanced thermoelectric performance observed in these hybrid films. Such a mobility gain is likely related to the morphology and structure of the PDI domains in the thin film. In light of this result, it is critical to understand the molecular ordering of PDI in the hybrid films.

2.3. Characterization of Crystal Structure and Molecular Level Ordering

In order to characterize the structure and packing of PDI molecules in the solid state, grazing-incidence wide angle X-ray scattering (GIWAXS) was performed on thin film samples consisting of 1) pure PDI, 2) pure S-Te NWs, and 3) composite PDI-Te NW films with varying PDI content. For this experiment, samples were prepared via Method A, and a wide range of PDI content (2–98 vol%) was investigated. While GIWAXS has been performed on films of these PDI molecules before, the complexity of the resulting spectra has impeded detailed crystallographic indexing until now.[15] Using high quality 2D GIWAXS data obtained using the Lawrence Berkeley National Laboratory (LBNL) Advanced Light Source (ALS) synchrotron, we report an explicit solution for the crystallographic structure of PDI molecules with high thermoelectric performance for the first time. This result enables more thorough understanding of the structural factors contributing to the high conductivity observed in PDI-Te hybrid nanostructures.

Structural studies have been performed on several similar small molecule systems, providing useful context for this work. In 2006, Guillermet et al. described the monoclinic crystal structure of a small molecule consisting of just the planar 3,4,9,10-perylene-tetracarboxylicacid diimide core.[37] Following reports observed similar monoclinic unit cells for crystals formed from planar PDI derivatives, while triclinic structures were observed in PDI molecules with alkyl side chains due to increased mobility and entanglement.[38,39] Klebe et al. observed a distorted triclinic unit cell in crystalline perylene-3,4:9,10-bis(dicarboximide), a molecule similar to the one presented in this report but with hydroxyl terminated side chains rather than amine terminated, indicating that functional side groups distort the unit cell further.[40] Commonalities in these reports include strong 001 and 002 reflections (representing end-to-end stacking of the PDI derivatives), "slipped" π–π stacking of the conjugated core, and significant (45–55°) angles between the substrate and the π–π stacking direction.

The 2D GIWAXS pattern presented in this work for pure PDI films is shown in **Figure 4**e. The pattern is consistent with previous reports, in which explicit indexing was not reported.[15] Here, we present a solution for the triclinic crystal structure observed in these materials, with the unit cell parameters summarized in **Table 2**. Upon geometric relaxation (using a Forcite package), these PDI molecules are observed to pack in a similar fashion to the analogous materials described previously (Figure 4f,g and Video S1, Supporting Information).[41] Additionally, an integrated and indexed 1D GIWAXS spectrum is presented in Figure S3 in the Supporting Information with a simulated XRD pattern further corroborating this result.

In the 2D GIWAXS spectrum (Figure 4e), the highest intensity peak is identified to be the (001) reflection, with a higher order (002) reflection clearly visible. The (001) peak represents the largest-scale molecular ordering in these films, with a periodicity of 26.0 Å, which has been attributed to the end-to-end distance across the long-axis of the PDI molecules (Figure 4f). Due to the tendency of the C_6 side chains to protrude from the PDI core at an angle (≈48°) and entangle via hydrophobic effects, this length scale is smaller than the end-to-end length of a fully extended PDI molecule (33.1 nm), similar to the observations made by Klebe et al. These peaks are anisotropically observed near the meridian (close to q_z), indicating a tendency to stack through-plane. Additionally, we observe slipped π–π stacking of these molecules, at an angle of 56.5° from the (001) plane. This corresponds to a 47.8° in reciprocal space, which matches the location of the (105) peak (π–π stacking direction) on the 2D GIWAXS detector. The similarities between our solution and those previously reported for molecules in this class

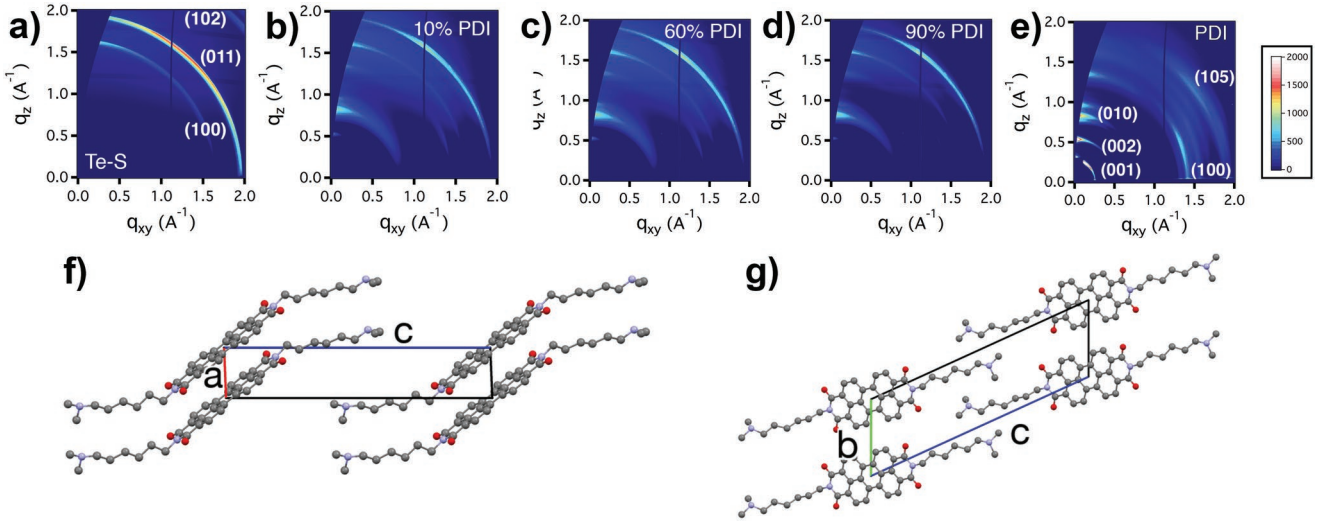

Figure 4. 2D GIWAXS performed on solid films of a) Te-S complex, b–d) Te-PDI composites of varying composition prepared via Method A, and e) pure PDI. In the low PDI regime, the GIWAXS spectra are dominated by the signal of the hexagonally packed Te crystal lattice. In the high PDI regime, the GIWAXS spectra feature peaks at lower q values corresponding to molecular packing and longer order organization of the PDI small molecules. The 2D GIWAXS data for pure PDI is used to solve the molecular crystal structure. f,g) Packing of PDI molecules into a unit cell is viewed along f) the *b*-axis and g) the *a*-axis. For ease of 3D visualization, an animation of the unit cell rotating is included in the Supporting Information as Video S1 in the Supporting Information.

Table 2. Unit cell parameters calculated for PDI crystal structure. The PDI crystallites exhibit triclinic structure with $Z = 2$ molecules per unit cell.

a [Å]	b [Å]	c [Å]
4.48	8.33	26.0
α	β	γ
65.4°	86.6°	86.8°

of materials, as well as the agreement between the calculated and observed peak locations (both q values and positions on the 2D detector) provide further evidence for the fitness of our solution.

GIWAXS spectra taken for S-Te NW thin films (Figure 4a) depict the expected hexagonal structure previously reported in a similar system (ICDD – PDF-4 #04-016-1605).[20] We note that the (100) peak is observed primarily near the meridian, and thus that the corresponding (100) plane is oriented primarily through-plane. Composite films of varying PDI content were also studied using GIWAXS (Figure 4b–d). Note that, in the moderate to low PDI regime, the Te (011) peak is convoluted with the PDI (105) peak. Of greatest import are the GIWAXS patterns observed for hybrid films in the high PDI regime, as this is the regime that demonstrates maximum thermoelectric performance. Interestingly, comparing the GIWAXS pattern for 100% PDI thin films to the 98% and 90% composite PDI-Te films reveals a shift in the peak of highest intensity. In pure PDI films, the (001) reflection is the most intense, whereas in the composite films, the (010) plane is dominant. This indicates a reorganization of PDI crystals on the Te surface relative to a bare substrate, likely tied to the increase in mobility implicated in the composite samples. In such a regime, the PDI π stack would tend to align along the surface of the inorganic nanostructure, likely leading to regions of high conductivity at the organic–inorganic interface. This result suggests that having a smooth, pristine inorganic surface onto which the PDI molecules can be templated during the PDI-Te composite formation is a critical component to producing high conductivity hybrid materials.

Further, it is possible to estimate the correlation length in the PDI crystallites using the Scherrer formula:

$$l = 2\pi K/\Delta q$$

where the Scherrer constant (K) is taken to be ≈0.9 and the correlation length (l) is calculated from the observed peak broadening (Δq).[15] In this way, we estimate the correlation length of PDI in thin films of 100%, 98%, and 90% PDI to be 84.5, 183, and 170 Å, respectively. The high conductivity PDI-Te composites demonstrate greater than twofold increase in correlation length. Again, the inorganic surface seems to play a role in templating larger crystalline domains of PDI at the organic–inorganic interface than are achieved in pristine PDI films. This result further corroborates the conclusion that structural reorganization of PDI molecules in the PDI-Te composites is tied to increasing thin film apparent electron mobility and thus thermoelectric performance of the hybrid system.

2.4. Composite Electronic Structure

Measurement of the WF and ionization energy (IE) for PDI-Te composites provides an important probe to understand the source of the high Seebeck coefficient observed in the hybrid nanostructures in the low PDI regime. For this goal, UPS was performed on thin films of varying PDI content; the results are summarized in Table 1, while the relevant spectra are depicted in Figure S4 in the Supporting Information. Additionally, the optical bandgaps of Te-S and PDI are calculated from Tauc plots (Figure S5, Supporting Information) to provide further details on the electronic structure of these materials. The Te-S complex has a WF within the narrow bandgap and located near the conduction band, as expected in an n-type semimetal. Pure PDI and the 90% PDI composite are shown to have a similar WF, although the bandgap is much larger in PDI than Te, as is typical with HOMO-LUMO gaps (gaps between the highest occupied molecular orbital and lowest unoccupied molecular orbital) in organic semiconductors. The 10% PDI complex has the greatest WF, in line with the EPR findings of relatively low carrier concentrations in the low PDI loading regime and corroborated by X-ray photoelectron spectroscopy (XPS) results (Figure S6, Supporting Information). This implies that the increase of Seebeck values measured in this low PDI regime are the result of dedoping of the system, likely due to localization of previously mobile carriers during formation of the composite.

2.5. Design of High-Performing PDI-Te Composites (Method B)

Using sulfur linkers (Method A) in preparing the PDI-Te composites provides an intuitive and flexible approach to the design of hybrid materials. Structural analysis of these materials reveals that the key to the improved thermoelectric performance observed in these materials is a templating effect, where the packing of PDI molecule is altered due to the presence of the inorganic nanostructure, likely due to an interaction between PDI molecules and the Te surface. This leads to a reorganization of PDI molecules in the hybrid films, as well as increased crystalline domain lengths. However, XPS reveals that much of the polyvinylpyrrolidone (PVP) ligand used in the original Te NW synthesis (Method A) is not removed during the S exchange process (Figure S7, Supporting Information). In order to promote templating of PDI molecules on the Te nanowire surface, it is desirable to have intimate contact between the organic and inorganic phases. Any residual PVP ligand and S linkers on the Te nanowire surface will likely reduce the surface area available for strong interaction between PDI and the Te surface, dampening the templating effects. Additionally, PVP and the S linkers are both electronic insulators, potentially reducing the electrical conductivities that can be achieved in films synthesized using this method. Driven by these conclusions, we demonstrate a second ligand exchange approach (Method B), in which much of the PVP ligands are removed via a stripping method, and PDI is coated directly onto the bare Te surface in a single-step procedure. Hydrazine hydrate was chosen as the stripping agent following literature precedent.[42,43] Hydrazine hydrate is a good candidate for this method because it is known to 1) efficiently strip hydrocarbon ligands from the surface of nanoparticles

without altering the nanoparticle size or shape, 2) act as a strong Lewis base to saturate any dangling bonds at the surface of the nanoparticles, 3) act as a reducing agent to repair any oxide defects at the nanoparticle surface, and 4) act as a Brönsted base to prevent ionized free ligands from reattaching to the nanoparticle surface.[43,44] Additionally, unlike the toxic and explosive anhydrous hydrazine, hydrazine hydrate procedures can be executed with minimal health risks in a standard fume hood. This procedure is used to enhance the templating effect of PDI on the Te surface, minimize the presence of insulating PVP and S moieties in the films, and simplify the composite preparation procedure from multistep to a single-step process. Thermogravimetric analysis (TGA) is used to confirm the removal of the majority of the hydrocarbon ligands from the Te nanowire surface (Figure S8, Supporting Information).

The composites prepared using Method B exhibit significantly improved electronic conductivity, demonstrating power factors up to 20 times greater than pure PDI and three orders of magnitude greater than the pure inorganic nanostructure (**Figure 5**). We note that the PDI-Te composites in the high PDI regime also achieve greater Seebeck coefficients than those composites prepared via Method A. The Seebeck coefficient is a complex function of several variables, including the carrier concentration, mobility, and density of states. Hydrazine hydrate treatment is known to alter the energetic landscape available to carriers at the organic–inorganic interface via reduction of oxide defects and filling of trap states, which likely contributes to the complex Seebeck coefficient trends observed. XPS spectra suggest stronger electronic coupling between the Te and PDI domains in composites prepared via Method B (Figure S9, Supporting Information). This result supports the conclusion that the interaction between organic molecules and inorganic nanostructure surfaces play a key role in the performance of hybrid thermoelectrics. Furthermore, this result showcases the potential of our methods and materials for preparing air stable, flexible n-type thermoelectric inks with high thermoelectric performance. Such materials are amenable to a host of solution-based processing techniques, enabling a variety of new thermoelectric device designs, from 2D-printed arrays to 3D flexible architectures. We provide proof of principle for this approach by demonstrating power generation in a flexible thermoelectric energy generator (TEG) using only our hybrid thermoelectric inks.

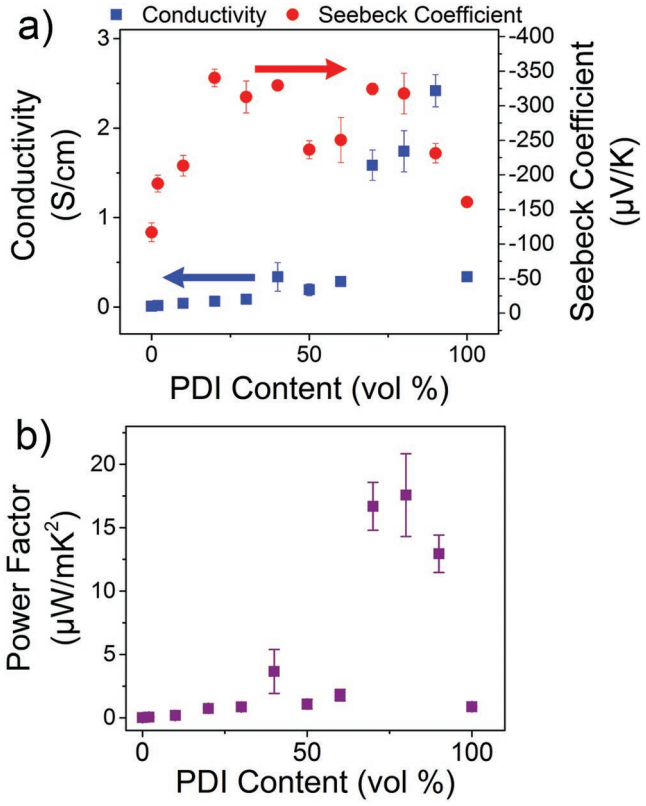

Figure 5. Thermoelectric transport properties measured for Te-PDI composites formed via hydrazine stripping, Method B. a) Similar nonmonotonic trends are observed in both Seebeck and electrical conductivity, implying that this technique provides a simplified, one-step route to make Te-PDI nanostructures with similar properties. b) Power factors achieved in this system are significantly greater than those in Method A, demonstrating up to 20× improvement in performance from pure PDI and three orders of magnitude improvement from the pure inorganic nanostructure.

2.6. Fabrication of Ink-Based Flexible Thermoelectric Generator

In order to test the viability of our all-solution-based approach, it is imperative to demonstrate realistic thermoelectric power generation in addition to measuring material properties. Here, we present the fabrication and characterization of flexible TEGs using a novel geometric design and facile, low-temperature solution-based techniques (detailed fabrication methodology provided in experimental section). Using a 10-leg device, the maximum power density generated was as large as 57 nW cm^{-2} (**Figure 6**d) under a small temperature gradient (50 K). This result is comparable to power generated in other flexible, soft material systems using only low temperature/low pressure solution-based techniques.[5,6,13] Mechanically, these devices demonstrated robust stability during flexing. The folded "stacked" geometry requires each leg to be flexed at both contact points. Traditional thermoelectric materials typically suffer from cracking or delamination in such geometries, whereas an all-ink design improves mechanical versatility and resiliency. Additionally, this design is modular in nature, and allows for simple modification of the number of legs connected in series. Thus, our approach enables new thermoelectric architectures for flexible power generation with low processing costs. This result represents a significant and promising proof-of-principle for all-ink, solution-processed flexible thermoelectrics.

3. Conclusions

To summarize, we have successfully demonstrated the preparation of novel n-type soft thermoelectric hybrids with high performance using PDI small molecules. We report the first explicit solution to the crystallographic structure of the PDI molecules in thin films, shedding new light into the relationship between structure and performance within this material class. Leveraging this new molecular level insight, a second methodology is

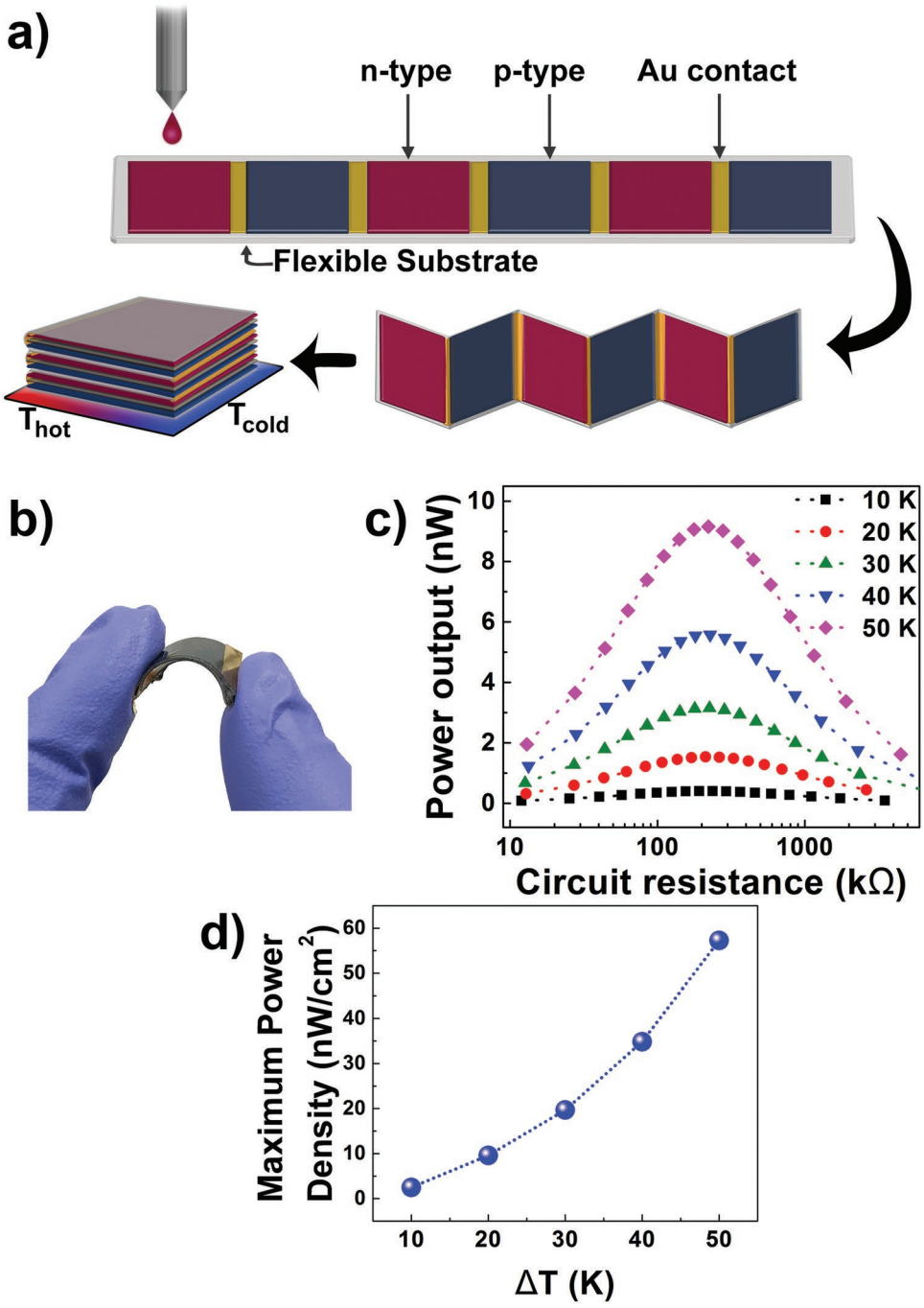

Figure 6. Flexible thermoelectric module design and performance. a) Using solution printing, a linear thermoelectric device is patterned onto a flexible substrate, which is then folded into a compact "stacked" structure. b) Photograph of 10-leg stacked TEG module demonstrating flexibility. c) Power density is measured as a function of load resistance at a variety of applied temperature gradients. d) Maximum power density observed is reported as a function of applied temperature gradients.

developed to prepare PDI-Te hybrid materials. Power factors as great as 17.6 μW mK^{-2} are achieved in this system, representing up to 20-fold improvement in thermoelectric performance over the pure PDI thin films. Detailed study of the energetics in this material system reveals that this phenomenon is the result of enhanced carrier mobilities, associated with the reorganization of the PDI molecules on the surface of the Te nanowires. This work provides strong evidence that ligand templating on inorganic nanostructures plays a crucial role in the electrical and thermoelectric transport of hybrid materials, marking the first experimental observation of this templating effect and corroborating recent theoretical work in the literature. This result adds critical insight into the mechanism of high performance in hybrid thermoelectric materials, a subject still under strong

debate. Finally, we report the fabrication of all-ink TEGs with impressive flexibility using a novel folded architecture. Since these materials use exclusively low temperature, facile solution processing, this approach represents a significant advantage for next-generation printed electronic devices.

4. Experimental Section

Materials: Tellurium dioxide (99.9995%), PVP (average molecular weight 55 kDa), sodium hydroxide (ACS reagent, ≥97.0%, pellets), ethylene glycol (ReagentPlus, ≥99%), hydrazine hydrate (78–82%, iodometric), sodium sulfide, and methanol (reagent grade, 98%) were purchased from Sigma-Aldrich. Acetone (J.T.Baker) and isopropyl alcohol (ACS grade) were purchased from VWR International. Ion exchange resin (Dowex Monosphere 550A hydroxide form, Sigma-Aldrich) was used to run a PDI counterion exchange column.

Composite Synthesis: Synthesis of PVP-capped Te nanowires (PVP-Te NWs) and surface exchange to sulfur-capped Te nanowires (S-Te NWs) followed existing literature procedures with slight modification.[15,17,23,30] Synthesis of PDI molecules and counterion exchange to hydroxyl have been previously reported. PDI-capped Te nanowires (PDI-Te NWs) were prepared via two ligand-exchange methods, Method A and Method B (details below). In both methods, PDI-Te NW solutions were then washed three times in methanol (9000 rpm, 45 min) to ensure a clean product of PDI-capped nanowires. During washing, the supernatant was yellow in hue, indicating removal of unbound PDI moieties. Finally, PDI-Te NWs were redispersed in water at a concentration of 20 mg mL^{-1}. The resulting solution was lustrous and silver, with a visible reddish hue indicative of the presence of PDI moieties on the surface of Te nanostructures. Transmission electron microscope (TEM) was used to visually confirm the presence of an organic PDI layer on the Te core, and to verify that the NWs maintain a high quality inorganic core of single crystalline Te (Figure 1c–e). XPS scans show a shift in the binding energy of the S 2p core levels upon addition of PDI, suggesting that the sulfur linkers interact electronically with the organic phase in the binding process (Figure S10, Supporting Information). These PDI-Te NWs were then used to prepare thin films. To prepare PDI loading ladders, PDI-Te NWs were mixed with varying amounts of additional PDI solution. It is important to note that capping the Te NW with PDI is crucial to the preparation of high quality composite films. Simply using a physical mixture of Te NWs and PDI results in phase separation, an indication of weakly interacting organic and inorganic phases. Scanning electron microscope (SEM) illustrates the film level organization (Figure S11, Supporting Information).

Method A: In the first method, sulfur (S) was used as a linker molecule to mediate binding between the Te and PDI domains (Figure 1a). In a typical reaction, 500 mg of precipitated S-Te NWs were collected, to which 5 mL of PDI solution (2 mg mL^{-1} in water) was added, and the mixture was then briefly vortexed followed by redispersion in 15 mL methanol.

Method B: In this method, hydrazine hydrate was used to partially strip the surface of PVP-Te NWs, destabilizing the nanostructures and allowing PDI to be directly coated onto the bare Te surface. In a typical reaction, 1.5 mmol of hydrazine hydrate were added to 200 mg of PVP-Te (concentration of 5 mg mL^{-1}) under vigorous stirring. The ligand stripping reaction was carried out for 30 min. If the reaction is allowed to progress too long (≈40 min), over-stripping of surface ligands will destabilize the nanostructures and cause the Te to crash out of solution. Afterward, the mixture was washed to remove hydrazine and unbound PVP (9000 rpm, 20 min). One milliliter of PDI solution (2 mg mL^{-1} in water) was added to the precipitate, and the mixture was then briefly vortexed followed by redispersion in 15 mL methanol.

Thin Film Preparation: Thin films were prepared via dropcasting on glass substrates (9.5 × 9.5 mm, 1 mm thick—Thin Film Devices). Substrates were pre-cleaned via sonication in three successive solvents, millipore water, acetone, and isopropanol, followed by nitrogen drying and UV-ozone treatment for at least 10 min. Clean substrates were placed on a large aluminum block acting as a thermal reservoir at 85 °C, and 75 µL of composite nanoparticle solution was dropcast onto the substrates. Films were partially covered to control evaporation and dried in this manner until all solvent had been removed (20–30 min).

Gold contacts for electrical measurements (100 nm thickness) were patterned onto each of the four corners of the dropcast films via thermal evaporation using a shadow mask. Identical experiments were carried out using bottom contacts (100 nm gold), but these samples demonstrated poor electrical contact in hybrid films with high inorganic loading. Cast films were annealed on a hot plate inside a nitrogen glovebox at 120 °C for 20 min before measurement and characterization. In previous reports on these PDI materials, annealing was shown to significantly improve the thin film electrical conductivity via a self-doping mechanism.[17] Quaternary ammonium cations were present on the PDI side chains in solution, which were converted to tertiary amines during the annealing process, which then act as powerful n-doping motifs coupled to the PDI core. The improved electrical conductivity and power factors after annealing was confirmed by measurement of PDI-Te thin film thermoelectric properties before and after the annealing step (Figure S12, Supporting Information).

Electrical and Thermoelectric Measurements: Sheet resistance of each film was measured using Keithley 2400 SourceMeters in 4-wire van der Pauw configuration. Film thickness was measured by scratching the film and measuring the step height with a Veeco Dektak 150 profilometer. Electrical conductivity was extracted from the sheet resistance and thickness measurements.

Seebeck coefficient (thermopower) was measured using a homemade probe setup. Two Peltier devices (Ferrotec) were placed ≈4 mm apart and a single current was passed through them in opposite polarities. This caused one device to heat and the other to cool approximately the same amount relative to room temperature. The sample was placed across these two devices such that a thermal gradient was established (thermal paste was used to ensure thermal contact—Wakefield Thermal S3 Solutions), and the resulting open circuit voltage was measured using an Agilent 34401 multimeter. The temperature gradient was measured using two T-type thermocouples mounted in micromanipulators. The magnitude of the temperature gradient was directly correlated to the amount of current driven through the Peltier devices. Typically, five different gradients were established (allowed to equilibrate for 200 sec between temperature changes), with ten voltage measurements taken and averaged at each ΔT. All samples exhibited linear variation of open circuit voltage with ΔT; this trend was used to extract Seebeck coefficient values. Data for both electrical conductivity and Seebeck coefficient were acquired using homemade LabVIEW programs. For each measurement, at least three different samples were measured and averaged, with error bars representing standard error. Ohmic contacts were confirmed before measurements. Hall mobilities were measured using an Ecopia HMS-5000 variable temperature Hall Effect Measurement System. Air stability measurements were also performed on the Ecopia system. PDI-Te hybrid films were prepared via Method A, and Te films were prepared via identical methodologies but without the addition of PDI. Both films were stored in ambient conditions and the conductivities were measured twice a day for 12 days. The air stability of the PDI-Te composite films appears to be significantly improved over films without PDI (Figure S13, Supporting Information).

Characterization of PDI-Te NWs and Thin Films: High resolution imaging of nanostructures and selected area electron diffraction (SAED) were acquired on a JEOL 2100-F field-emission analytical TEM at an accelerating voltage of 200 kV. TEM samples were prepared on grids of 400-mesh Cu or Ni on holey carbon (Ted Pella 01824). Thin film imaging was performed on a Zeiss Gemini Ultra-55 analytical field emission SEM using a beam energy of 5 kV. TGA was performed on a TA Instruments Q5500 TGA to quantify organic–inorganic composition of each sample. Seven to ten milligrams of each sample was ramped to 600 °C at a scan rate of 5 °C min^{-1} and held there for 120 min. The weight lost was assumed to be the organic content of the hybrid, and the remaining weight was taken to be the inorganic content.

Spin quantification was performed at room temperature using EPR on a Varian E109 EPR spectrometer equipped with a Model 102 Microwave bridge. The following spectrometer conditions were used: microwave

frequency: 9.22 GHz; field modulation amplitude: 32 G at 100 kHz; microwave power: 20 mW. Quantification was performed according to existing literature standards using the stable free radical 1,1-diphenyl-2-picrylhydrazyl (DPPH) as a standard.[17,34–36] Samples and standard were dropcast onto quartz microscope cover slides and cleaved into pieces roughly 2–4 mm in dimension. Samples were inserted into quartz EPR tubes and sealed with vacuum grease and plastic caps. Triplicates were measured at every PDI loading level analyzed. All samples and standards were measured within 4 h of preparation. Spin quantities were determined by comparing the EPR signals from PDI-Te samples to those of the DPPH samples with known spin quantities using the following equation:

$$\frac{N_1}{N_2} = \frac{\left(a \times \Delta H_{pp}^2\right)_1}{\left(a \times \Delta H_{pp}^2\right)_2}$$

where a is the peak-to-peak derivative amplitude and ΔH_{pp} is the peak-to-peak line width. Profilometry was used to measure film thickness to calculate per volume spin concentrations.

2D GIWAXS was performed at the LBNL ALS on beamline 7.3.3 with an area detector, a camera length of ≈25–30 cm, and an incident energy of 10 keV. Films were typically exposed for 60 s at an incidence angle of 0.10°. Acquired images were normalized with a AgB standard.

XPS and UPS were performed on a Thermo K-Alpha Plus instrument with a monochromatic Al X-ray source. For high resolution scans, the pass energy was set to 20 eV and the energy resolution to 0.1 eV. UPS was performed using a He I source at 21.2 eV. Thin film surfaces were cleaned using an Ar cluster gun (6000 eV per cluster, 150 atoms per cluster, 15 sec) before all UPS experiments.

UV–vis–NIR spectroscopy was performed on a Cary 5000 instrument in absorbance mode with a range of 190–3300 nm.

Thermoelectric Module Design and Performance: TEGs were prepared simply using solution-based techniques and a novel, modular design (Figure S14, Supporting Information). A flexible polyethylene terephthalate (PET, 0.0005 in. thickness—McMaster-Carr) substrate was patterned with gold electrodes (100 nm thick) using thermal evaporation. The substrates were then UV-ozone treated to improve hydrophilicity followed by dropcasting of the hybrid thermoelectric inks at 75 °C. On a single substrate, 3–4 p–n couples were deposited to form a thermoelectric module, and several modules were connected in series to form a thermoelectric device with the desired number of p–n legs. The modules were then folded along the gold electrodes to produce a TEG with a stacked geometry (Figure 6 and Figure S9, Supporting Information). For the n-type leg, the PDI-Te nanowire composite was used, while for the p-type leg, a well-studied PEDOT:PSS-Te nanowire composite was used.[8–10] The p-type material was chosen due to its analogous inorganic nanostructure, ease of synthesis, high thermoelectric performance, and air stability. The TEG was then suspended across two hot Peltier devices and connected to a Keithley 2400 SourceMeter. Each Peltier was operated separately to produce thermal gradients ranging from 10 to 50 K. At a given temperature gradient, the SourceMeter was used to apply varied electrical currents and measure the resulting module resistances. These measurements were used to identify the optimal operating condition at each temperature gradient and to calculate the maximum power generated there. All measurements were performed in air.

Supporting Information

Supporting Information is available from the Wiley Online Library or from the author.

Acknowledgements

This work was performed at the Molecular Foundry and Advanced Light Source, Lawrence Berkeley National Laboratory, and was supported by the Department of Energy, Office of Science, Office of Basic Energy Sciences, Scientific User Facilities Division of the U.S. Department of Energy under Contract No. DE-AC02-05CH11231. EPR studies were performed with support of the Office of Science, OBES, Division of Chemical Sciences, Geosciences, and Biosciences (CSGB) of the DOE under contract no. DE-AC02-05CH11231 (J.Y.). E.W.Z. and M.P.G. gratefully acknowledge the National Science Foundation for fellowship support under the National Science Foundation Graduate Research Fellowship Program. The authors acknowledge Professor Craig Hawker and Dr. Brenden McDearmon, supported by NSF DMR 1436263, for the PDI synthesis reported in this paper.

Conflict of Interest

The authors declare no conflict of interest.

Keywords

hybrid, n-type, organic–inorganic, perylene diimide, thermoelectric

Received: November 9, 2018
Revised: January 14, 2019
Published online:

[1] B. Russ, A. Glaudell, J. J. Urban, M. L. Chabinyc, R. A. Segalman, *Nat. Rev. Mater.* **2016**, *1*, 16050.
[2] Y. Chen, Y. Zhao, Z. Liang, *Energy Environ. Sci.* **2015**, *8*, 401.
[3] J.-H. Bahk, H. Fang, K. Yazawa, A. Shakouri, *J. Mater. Chem. C* **2015**, *3*, 10362.
[4] J. J. Urban, *Nat. Nanotechnol.* **2015**, *10*, 997.
[5] T. Varghese, C. Hollar, J. Richardson, N. Kempf, C. Han, P. Gamarachchi, D. Estrada, R. J. Mehta, Y. Zhang, *Sci. Rep.* **2016**, *6*, 33135.
[6] C. A. Hewitt, A. B. Kaiser, S. Roth, M. Craps, R. Czerw, D. L. Carroll, *Nano Lett.* **2012**, *12*, 1307.
[7] P. Fan, Z. Zheng, Y. Li, Q. Lin, J. Luo, G. Liang, X. Cai, D. Zhang, F. Ye, *Appl. Phys. Lett.* **2015**, *106*, 073901.
[8] T. O. Poehler, H. E. Katz, *Energy Environ. Sci.* **2012**, *5*, 8110.
[9] C. Badre, L. Marquant, A. M. Alsayed, L. A. Hough, *Adv. Funct. Mater.* **2012**, *22*, 2723.
[10] O. Bubnova, Z. U. Khan, A. Malti, S. Braun, M. Fahlman, M. Berggren, X. Crispin, *Nat. Mater.* **2011**, *10*, 429.
[11] O. Bubnova, X. Crispin, *Energy Environ. Sci.* **2012**, *5*, 9345.
[12] Y. Sun, P. Sheng, C. Di, F. Jiao, W. Xu, D. Qiu, D. Zhu, *Adv. Mater.* **2012**, *24*, 932.
[13] C.-K. Mai, B. Russ, S. L. Fronk, N. Hu, M. B. Chan-Park, J. J. Urban, R. A. Segalman, M. L. Chabinyc, G. C. Bazan, *Energy Environ. Sci.* **2015**, *8*, 2341.
[14] K. Shi, F. Zhang, C.-A. Di, T.-W. Yan, Y. Zou, X. Zhou, D. Zhu, J.-Y. Wang, J. Pei, *J. Am. Chem. Soc.* **2015**, *137*, 6979.
[15] B. Russ, M. J. Robb, F. G. Brunetti, P. L. Miller, E. E. Perry, S. N. Patel, V. Ho, W. B. Chang, J. J. Urban, M. L. Chabinyc, C. J. Hawker, R. A. Segalman, *Adv. Mater.* **2014**, *26*, 3473.
[16] R. J. Chesterfield, J. C. McKeen, C. R. Newman, P. C. Ewbank, D. A. da Silva Filho, J.-L. Brédas, L. L. Miller, K. R. Mann, C. D. Frisbie, *J. Phys. Chem. B* **2004**, *108*, 19281.
[17] B. Russ, M. J. Robb, B. C. Popere, E. E. Perry, C.-K. Mai, S. L. Fronk, S. N. Patel, T. E. Mates, G. C. Bazan, J. J. Urban, M. L. Chabinyc, C. J. Hawker, R. A. Segalman, *Chem. Sci.* **2016**, *7*, 1914.
[18] E. S. Cho, N. E. Coates, J. D. Forster, A. M. Ruminski, B. Russ, A. Sahu, N. C. Su, F. Yang, J. J. Urban, *Adv. Mater.* **2015**, *27*, 5744.

[19] L. Wang, Z. Zhang, L. Geng, T. Yuan, Y. Liu, J. Guo, L. Fang, J. Qiu, S. Wang, *Energy Environ. Sci.* **2018**, *11*, 1307.
[20] H. Imai, Y. Shimakawa, Y. Kubo, *Phys. Rev. B* **2001**, *64*, 241104.
[21] K. C. See, J. P. Feser, C. E. Chen, A. Majumdar, J. J. Urban, R. A. Segalman, *Nano Lett.* **2010**, *10*, 4664.
[22] E. J. Bae, Y. H. Kang, K.-S. Jang, S. Y. Cho, *Sci. Rep.* **2016**, *6*, 18805.
[23] A. Sahu, B. Russ, N. C. Su, J. D. Forster, P. Zhou, E. S. Cho, P. Ercius, N. E. Coates, R. A. Segalman, J. J. Urban, *J. Mater. Chem. A* **2017**, *5*, 3346.
[24] L. Wang, Z. Zhang, Y. Liu, B. Wang, L. Fang, J. Qiu, K. Zhang, S. Wang, *Nat. Commun.* **2018**, *9*, 3817.
[25] E. W. Zaia, A. Sahu, P. Zhou, M. P. Gordon, J. D. Forster, S. Aloni, Y.-S. Liu, J. Guo, J. J. Urban, *Nano Lett.* **2016**, *16*, 3352.
[26] N. E. Coates, S. K. Yee, B. McCulloch, K. C. See, A. Majumdar, R. A. Segalman, J. J. Urban, *Adv. Mater.* **2013**, *25*, 1629.
[27] P. Kumar, E. W. Zaia, E. Yildirim, D. V. M. Repaka, S.-W. Yang, J. J. Urban, K. Hippalgaonkar, *Nat. Commun.* **2018**, *9*, 5347.
[28] Z. Liang, M. J. Boland, K. Butrouna, D. R. Strachan, K. R. Graham, *J. Mater. Chem. A* **2017**, *5*, 15891.
[29] J. Vura-Weis, M. A. Ratner, M. R. Wasielewski, *J. Am. Chem. Soc.* **2010**, *132*, 1738.
[30] G. Zhang, B. Kirk, L. A. Jauregui, H. Yang, X. Xu, Y. P. Chen, Y. Wu, *Nano Lett.* **2012**, *12*, 56.
[31] J. P. Heremans, V. Jovovic, E. S. Toberer, A. Saramat, K. Kurosaki, A. Charoenphakdee, S. Yamanaka, G. J. Snyder, *Science* **2008**, *321*, 554.
[32] T. H. I. Reilly, A. W. Hains, H. Y. Chen, B. A. Gregg, *Adv. Energy Mater.* **2012**, *2*, 455.
[33] B. A. Gregg, R. A. Cormier, *J. Phys. Chem. B* **1998**, *102*, 9952.
[34] D. T. Burns, B. D. Flockhart, *Philos. Trans.: Phys. Sci. Eng.* **1990**, *333*, 37.
[35] U. Hochkirch, W. Herrmann, R. Stößer, K.-P. Moll, J. G. Llerena, M. Linscheid, H.-H. Borchert, *Appl. Magn. Reson.* **2008**, *35*, 173.
[36] N. D. Yordanov, *Appl. Magn. Reson.* **1996**, *10*, 339.
[37] O. Guillermet, M. Mossoyan-Déneux, M. Giorgi, A. Glachant, J. C. Mossoyan, *Thin Solid Films* **2006**, *514*, 25.
[38] A. L. Briseno, S. C. B. Mannsfeld, C. Reese, J. M. Hancock, Y. Xiong, S. A. Jenekhe, Z. Bao, Y. Xia, *Nano Lett.* **2007**, *7*, 2847.
[39] S. Tatemichi, M. Ichikawa, T. Koyama, Y. Taniguchi, *Appl. Phys. Lett.* **2006**, *89*, 112108.
[40] G. Klebe, F. Graser, E. Hädicke, J. Berndt, *Acta Crystallogr., Sect. B: Struct. Sci., Cryst. Eng. Mater.* **1989**, *45*, 69.
[41] N. Iwamoto, M. M. F. Yuen, H. Fan, *Molecular Modeling and Multiscaling Issues for Electronic Material Applications*, Springer Science & Business Media, NY **2012**.
[42] M. Scheele, N. Oeschler, K. Meier, A. Kornowski, C. Klinke, H. Weller, *Adv. Funct. Mater.* **2009**, *19*, 3476.
[43] M. V. Kovalenko, M. Scheele, D. V. Talapin, *Science* **2009**, *324*, 1417.
[44] D. V. Talapin, C. B. Murray, *Science* **2005**, *310*, 86.